Visualization of Noisy and Less Noisy Computational Basis States in Quantum Computing

1st Priyabrata Senapati
dept. Computer Science
Kent State University
Kent, USA
psenapat@kent.edu

2nd Qiang Guan
dept. Computer Science
Kent State University
Kent, USA
qguan@kent.edu

3rd David Pugmire
Oak Ridge National Lab
Oak Ridge, USA
pugmire@ornl.gov

4th Cheng Chang Lu
Qradle Inc.
clu@kent.edu

5th Tushar M. Athawale
Oak Ridge National Lab
Oak Ridge, USA
athawaletm@ornl.gov

***Abstract*—Quantum computing technology holds substantial promise as a reliable computational paradigm. However, current noisy intermediate scale quantum (NISQ) systems, are significantly impacted by noise originating from hardware inconsistencies. This noise causes errors and lowers output fidelity. So we must find which basis states cause errors. However, there are two main challenges in analyzing noise corresponding to basis states. First, the noise distribution data is high dimensional in nature, thereby making its analysis challenging. Second, although functional box plots have been used in the state of the art research to understand such a high dimensional data, they suffer from clutter and occlusion issues because of overplotting. In this study, we introduce an innovative visualization pipeline to address the aforementioned challenges to provide a clear depiction of noisy and less-noisy basis states. Specifically, our proposed visualization pipeline comprises three stages namely, low dimensional embedding, clustering, and violin plot visualization, to reduce visual clutter and effectively analyze high-dimensional noise distribution data. Our analysis uses quantum machine learning (QML) circuits as case study for drawing a distinction between noisy and less noisy basis states.**

***Index Terms*—quantum computing, variational quantum algorithm, quantum machine learning, quantum computers noise, visualization, violin plots, clustering, manifold embedding, Kullback–Leibler divergence**

I. Introduction

In this paper, we present a new visualization approach to study noise in quantum computing systems. Quantum computers promise exponential or quadratic speed-ups for classically intractable tasks, such as Shor's algorithm for integer factorization [24] and Grover's algorithm for unstructured search [6]. Yet today's noisy intermediate-scale quantum (NISQ) processors introduce stochastic errors that erode fidelity and reproducibility [22], [23]. Thus, understanding and ultimately mitigating such noise remains a first-order obstacle to quantum advantage. Noise in NISQ devices stems from a variety of reasons, including inaccurate microwave pulses [10], qubit-qubit crosstalk [20], [25], and readout errors [1], [14], [7], introduced by classical electronics. Furthermore, temporal drift compounds the noise problem; accuracies fluctuate across days [22], [23], and distance metrics such as the time varying Hellinger distance reveal non-stationarity [5]. Analyzing noise in *quantum basis states* is, therefore, crucial to understanding which basis states contribute more to output noise [23]. Quantum basis states essentially represent the orthonormal vectors ($|0\rangle$) and ($|1\rangle$) for a single qubit, and their tensor product combinations (e.g. ($|00\rangle$, $|01\rangle$, $|10\rangle$, $|11\rangle$) for two qubits that serve as reference axes for expressing any quantum state via linear combination of these vectors called superposition. In this work, we propose a novel visualization pipeline to help users understand noisy and less-noisy basis states and their noise distributions.

Visualization has become an indispensable tool [16]–[19] for understanding, and ultimately mitigating the complexities of near term quantum devices. Brahmbhatt et al. [3] introduced QubiCSV, an open source platform that supports real time, collaborative management, versioning, and visualization of large-scale qubit calibration data, thereby reducing experimental cost and complexity. To diagnose the performance bottlenecks that arise after calibration, VACSEN by Ruan et al. [18] employs coordinated views to reveal how hardware and circuit noise erode quantum speedups. More broadly, Li et al. [13] proposed a quantum data visualization framework that harnesses quantum effects and geometric primitives to generate interactive 2D and 3D summaries, such as circuit based pie charts, scatter plots, and bar graphs while minimizing resource overhead. Richter's 3D phase space slices for 4D symplectic maps [15] likewise advance the comparison of chaotic and regular dynamics beyond conventional techniques.

Complementary efforts have focused on representing quantum basis states themselves, ranging from Bloch sphere inspired 2D glyphs for small systems [19] to BEADS phase space diagrams that simplify multi level behavior [9]. Preliminary work has also begun to visualize noise in quantum machine learning (QML) settings, most notably functional boxplots [21], but these overlays of median, quantile, and outlier curves often suffer from occlusion and clutter, obscuring noisy versus less-noisy basis states (see Figure 2a (i)). Building directly on this prior study, our work proposes a new visualization suite that overcomes the limitations of functional box plots and enables clear, scalable exploration of high-dimensional NISQ-era basis-state data, thereby making noise patterns in QML applications

both discernible and communicable to end users.

In the absence of extraneous noise beyond shot noise, the true probability of each basis state remains constant and correlates directly with the square of its amplitude in the quantum superposition. However, the introduction of additional noise types can distort these probabilities, impacting the prepared quantum superpositions. This probabilistic nature of quantum measurements contrasts sharply with the deterministic nature of classical computing, leading to variability in outputs. Our objective is to systematically explore and visualize the variations and associated noise in basis state probabilities that result from errors caused by system-environment coupling and multiple gate operations, through a collective analysis of qubit-related errors.

We propose a novel visualization to overcome the limitations approach proposed in [21] to elucidate quantum basis states, the fundamental computational units generated by n qubits. For example, a system comprising 7 qubits can produce $2^7 = 128$ distinct computational basis states. To estimate the probability of observing a specific basis state, we repeatedly prepare and measure the quantum state; each measurement collapses the quantum superposition, revealing only a singular basis state at a time. By aggregating the frequency of occurrences for each basis state, we can derive probability estimates, with the estimation error diminishing as the number of measurements increases, a phenomenon known as shot noise [4].

In this paper, we designed our methodology with a particular emphasis on addressing the variability produced by noise in quantum computers. Notably, the activation of basis states is influenced by two distinct factors. First, noise induced errors can inadvertently result in the activation of extraneous basis states. Second, the inherent variability in pixel intensities across MNIST images, even among those within the same class that naturally leads to a diverse pattern of activated basis states. Consequently, attributing the observed variability solely to quantum noise does not adequately capture the intrinsic heterogeneity of the image data. We contend that our approach is capable of encompassing both types of variability, thereby offering a comprehensive framework for analyzing the effects of noise and natural data variation in quantum computing applications.

In our study, we focus on classifying quantum states by analyzing their corresponding images. Specifically, our methodology involves collecting multiple images for each distinct class of quantum states. By doing so, we can capture a comprehensive range of basis state amplitudes within each class. This approach allows us to effectively represent the variability and complexity inherent in each quantum state category, facilitating more accurate classification and analysis. This variability is beneficial and will be retained even in advanced, noiseless quantum architectures. However, temporal noise introduces uncertainty that can adversely affect the output of quantum circuits. Thus, it is preferable to analyze all images within a class rather than relying on a singular image, as this approach more accurately represents the influence of temporal noise on our uncertainty visualizations while minimizing the effects of pixel value variations.

We utilize violin plots to depict basis state uncertainty. Violin plots combine elements of box plots and density plots to illustrate the distribution of a dataset [8]. They present the probability density function of the data across varying values, employing kernel density estimation to create a smooth, mirrored shape reminiscent of a violin. This visualization provides a comprehensive overview of the data distribution, highlighting central tendencies, dispersion, and the presence of multiple modes [8]. Each ”violin” represents distinct groups or categories, enabling intuitive comparisons of data distributions across multiple cohorts. By showcasing both the density and summary statistics (such as the median and quartiles), violin plots offer a detailed and informative representation of data variability and structure [8].

Violin plots have emerged as a powerful alternative to traditional boxplots for visualizing data distributions, particularly in complex scenarios encountered in quantum machine learning. While boxplots summarize central tendency and dispersion through medians, quartiles, and outlier detection, they often mask deeper distributional features such as multimodality, skewness, and subtle density variations. They overcome these limitations by integrating kernel density estimation with conventional boxplot elements, thereby revealing the full shape of the underlying data. In our work, we harness the expressive power of violin plots to capture the complexities inherent in distinguishing between noisy and less noisy basis states.

For example, in Figure 2c (i), the basis states corresponding to cluster centroid 61 display a high median alongside considerable variance suggesting that these noisy states are activated frequently but with inconsistent occurrence, which leads to a degree of instability. In contrast, basis states associated with cluster centroid 117 exhibit both a low median and low variance, indicative of less noisy behavior where activations occur more consistently, thereby ensuring greater stability. This observation underscores a central tenet of our approach: while noisy basis states may fire with a relatively high probability, the lack of consistency in their occurrence results in unstable measurement outcomes, whereas less noisy basis states, despite a similar activation probability, do so uniformly, leading to stable behavior. By leveraging violin plots, our methodology not only captures these nuanced distinctions but also provides a robust framework for analyzing and interpreting the effects of any noise whether that noise is intrinsic to quantum systems or originates from variability in the input data used with these systems to drive deeper insights into quantum machine learning applications

We design a visualization pipeline comprising three steps to overcome shortcomings of functional box plots. Specifically, high dimensional basis state noise distributions are (i) embedded into a low-dimensional space to preserve distributional symmetry, (ii) clustered to group basis states with similar noise distributions, and (iii) summarized via violin plots that reveal shape and spread of noise distribution. This pipeline suppresses overplotting yet retains the full distributional story of noise in basis states.

This paper is not primarily a quantum error mitigation(QEM) study; rather, it emphasizes the role of visualization techniques in depicting both noisy and less-noisy basis states and demonstrates how these techniques can play a crucial role in revealing the

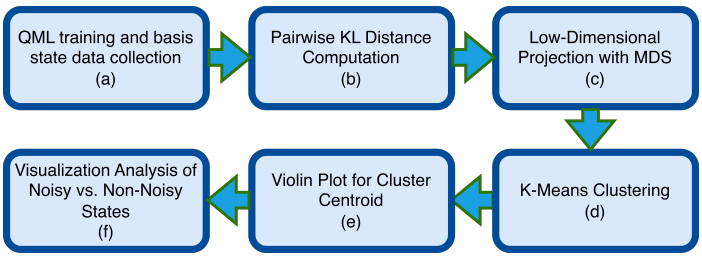

Fig. 1: Our proposed pipeline for visualizing noise in quantum basis states comprises: (a) collecting high-dimensional raw data representing noise in the basis state probabilities for a 7-qubit system, (b) calculating pairwise KL distances between noise distributions of the basis states, (c) projecting the $r \times 128$ matrix (with $r = 8000$) to a 2×128 matrix through low-dimensional embedding using MDS with KL metrics, (d) deriving clusters in the low-dimensional space from the 128 basis states using k-means clustering, (e) plotting the cluster centroid noise distributions with violin plots, and (f) visualizing the noisy and less-noisy basis states.

noise characteristics inherent in quantum systems. Although our proposed visualizations can inform future quantum error mitigation schemes by enabling users to identify the quality of qubits, this work focuses on diagnostic insight and does not propose new error mitigation algorithms. Our study relies on legacy systems, a necessity imposed by an extensive data collection period that spanned nearly 20 months due to stringent backend usage and access restrictions, and in light of rapid advancements in IBM's quantum processor technology that have since rendered many of these systems obsolete, underscores the challenges inherent in aligning long term data acquisition with rapidly evolving hardware platforms. The main contribution of this work lies in providing an insightful and innovative framework for visualizing basis-state behavior under varying noise conditions. In summary, our contributions are as follows.

- We present a noise-aware visualization pipeline that embeds, clusters, and summarizes high-dimensional basis-state noise distribution data, enabling rapid identification of noisy and less-noisy basis states.
- We demonstrate substantial reductions in occlusion and visual clutter relative to the state-of-the-art functional box plot approach [21] by using our visualization pipeline.
- We demonstrate our proposed visualizations against the functional boxplot approach using 7-qubit QML applications on three IBM quantum computers (Lagos, Perth, and Nairobi).

II. Methodology

Our methodology for collecting and visualizing the distribution of basis states is structured into a series of six systematic steps, as illustrated in the flowchart in Figure 1. (1) We begin by training our quantum machine learning (QML) algorithm [23] to facilitate the collection of raw data, from which we derive the noise distribution for the basis states (Figure 1a). (2) Next, we quantify the pairwise distances between distributions for all basis states using the Kullback-Leibler (KL) divergence metric (Figure 1b). (3) We then apply multidimensional scaling (MDS) [12] to achieve low-dimensional embeddings of the high-dimensional error distributions associated with each basis state (Figure 1c). (4) Subsequently, we compute K clusters in the projected space utilizing the k-means clustering algorithm (Figure 1d). (5) To represent the noise distribution of the cluster centroids, we employ violin plots [8] (Figure 1e). (6) Finally, we visualize both noisy and less noisy basis states within the projected space(Figure 1f).

(1) **QML Training:** We commence by training and evaluating a quantum machine learning (QML) algorithm [23] for the classification of MNIST images corresponding to the classes 3, 6, and 9. This task is illustrated in Figure 1(a). The selection of these specific classes is arbitrary; other classes could have been chosen as well. The original 28×28 pixel images are downscaled to 12×12 pixels to align with the amplitude requirements of the 7-qubit quantum computers utilized in our experiments. This downscaling is achieved through 2D adaptive average pooling applied to an input signal comprising multiple input planes. Training is conducted on a noisy quantum computer simulator that emulates the Noisy Intermediate-Scale Quantum (NISQ) devices employed in our study. The training dataset consists of 2000 images, selected for simulation due to restrictions imposed by IBM Quantum's fair share job scheduling algorithms on actual quantum hardware.

The training regimen involves conducting model training on one designated day each week, followed by testing on the remaining six days across various quantum machines, contingent upon the job execution wait times associated with cloud-based quantum computing. Model accuracy is assessed on three distinct devices: IBM Nairobi, IBM Lagos, and IBM Perth. A critical aspect of our methodology involves excluding MNIST images from the test set that have been inaccurately classified by our noise-free simulator. This technique enables us to achieve 100% test accuracy with the noise-free simulator. Consequently, only these accurately predicted test images are utilized for predictions on actual quantum computers. Concurrently, these selected images are employed for testing on noisy quantum computers, thereby eliminating noise originating from the test images and allowing for the documentation and visualization of noise attributable solely to the quantum hardware. The testing procedure entails evaluating 300 images from a single batch, corresponding to the aforementioned image classes. We submit batches of images as jobs to the IBM Quantum cloud as frequently as possible throughout the six-day testing period.

(2) **Raw Data Collection:** The 2D test image data is converted into quantum circuits prior to compilation for execution on the quantum computer. The outputs of the circuits corresponding to the model accuracy assessments are collected from all three devices (IBM Lagos, IBM Nairobi, and IBM Perth) utilized in our workflow. The raw output data, represented as distributions of basis states, is extracted from the executed jobs across all quantum computers involved in our study. This data collection is facilitated by our custom-built crawler for executed quantum circuit jobs. Once the raw data is acquired, yielding a probability

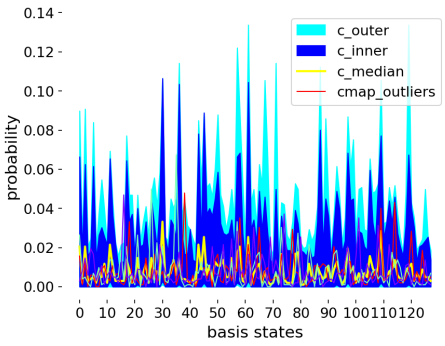

(a (i)) Functional boxplot of raw data

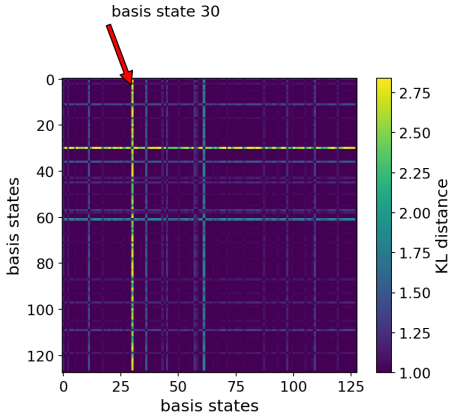

(a (ii)) Pairwise KL-distance for all jobs

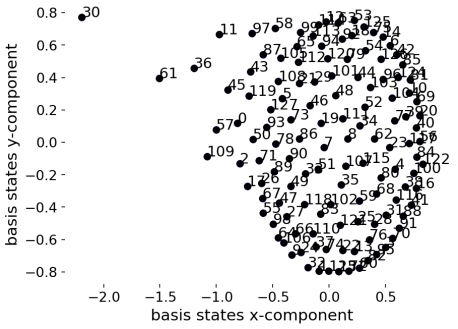

(a (iii)) Low-dimensional projection of basis states with MDS

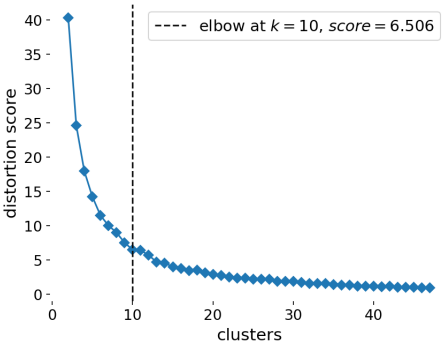

(b (i)) k-means elbow plot with distortion metric

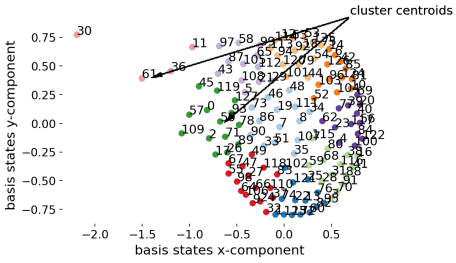

(b (ii)) Basis states divided among 10 clusters

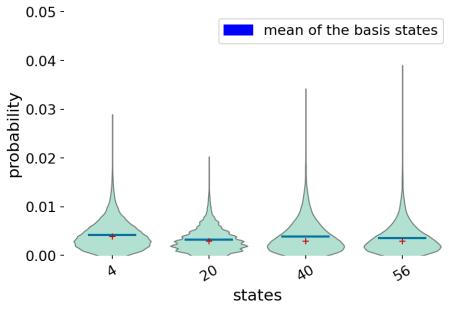

(b (iii)) Four states from a same cluster

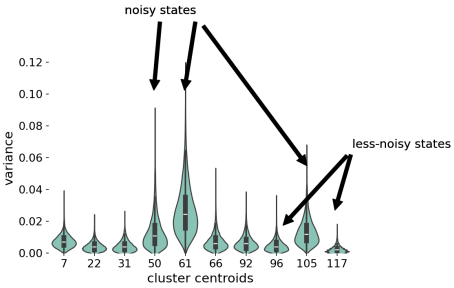

(c (i)) Violin plots for cluster centroids

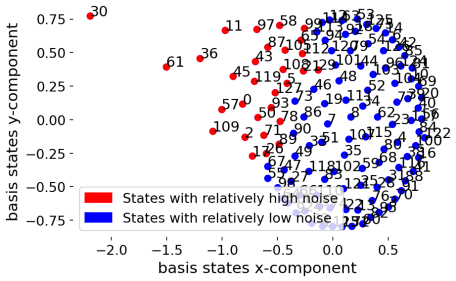

(c (ii)) Clusters divided between noisy and less noisy groups w.r.t to c(i)

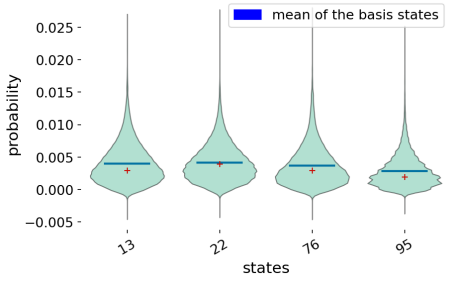

(c (iii)) Four states from the cluster with centroid 22 have similar shapes

Fig. 2: IBM Lagos: The sequence used in our methodology for finding the noisy quantum states is $(a(ii)) \rightarrow (a(iii)) \rightarrow (b(i)) \rightarrow (b(ii)) \rightarrow (c(i)) \rightarrow (c(ii))$. The proposed visualizations in c(i)-(ii) provide insight into noisy and less-noisy basis states with lesser visual clutter compared to the functional box plot in a(i). The proposed violin plots in (c(i)) show detailed noise distribution, which is not observable in functional box plots. Furthermore, our violin plot method in c(i) demonstrates enhanced clarity and reduced visual clutter compared to a(i), as it depends on the number of cluster centroids rather than the number of basis states. Additionally, the scatterplot presented in c(ii) offers a more comprehensive depiction of noisy (red) versus less-noisy (blue) basis states.

distribution across all $(2^7 = 128)$ quantum computational basis states, we populate the non-involved basis states in the test dataset predictions with zeros. A total of 8000 executed circuits are analyzed from IBM Perth, IBM Lagos, and IBM Nairobi for this data collection.

The raw data constitute an $r \times 128$ matrix ($r = 8000$) generated by our crawler script, which converts Qiskit's [11] shot count outputs after compiling and executing the 2D test image circuits on IBM Lagos, Perth, and Nairobi. Each row, one per test image from a single MNIST class contains the empirical probability distribution across the $2^7 = 128$ basis states of the 7-qubit register; unused states are padded with zeros. Consequently, every basis state is assigned 8000 probability values, capturing the noise in the measurement outcomes and yielding the output distribution needed to infer results for all 8000 images.

In a perfect, noise free quantum setting, running the circuit and measuring it should return one definite basis state, since measurement collapses the superposition to a single outcome. However, due to the inherent noise present in quantum computing, the observed outcomes frequently include unexpected basis states or superpositions that diverge from the anticipated noiseless states. Consequently, when interpreting the prediction outputs from noisy quantum computers, it is common to encounter scenarios where the probabilities of multiple basis states are neither strictly zero nor one, even though the ideal prediction should correlate to a single basis state with a probability of one.

In our case, with 8000 executed circuits, we generate a raw data matrix of size (8000×128) (where $r = 8000$). Our objective is to assess the extent of variation or noise across the r rows for each basis state. If significant variation is observed across the r rows for a particular basis state, that state is classified as a "noisy" basis state. To facilitate the identification and understanding of noisy versus less noisy basis states within the raw data, we propose a novel visualization pipeline, wherein each column of the raw data represents a high-dimensional noise representation (i.e., $r = 8000$).

(3) **Functional Box Plot Visualization:** Variation in the probability distributions of basis states across the r rows of raw data can be displayed with functional box plots [21]. As illustrated in Figure 2a (i), the plot encodes the central 50% of the distribution in dark blue (c_{inner}), the outlier region in red (c_{outer}), and the median curve in yellow (c_{median}) for 128 basis states, i.e., a 7-qubit system. Unfortunately, on such high dimensional data the functional box-plot becomes visually cluttered and offers limited clarity, masking the distinctions between noisy and less-noisy basis states. To remedy this, we introduce a new visualization pipeline explicitly designed to reduce clutter, sharpen differentiation, and provide a more comprehensive and insightful analysis.

(4) **Pairwise KL Distance (Figure 1b):** To assess how similar the noise distributions are for every pair of computational basis states, we begin with the raw data matrix of size $r \times 128$ ($r = 8000$; see Figure 1b). For each of the 128 columns we build a histogram that captures its noise distribution, then compute the Kullback–Leibler (KL) divergence between every pair of these

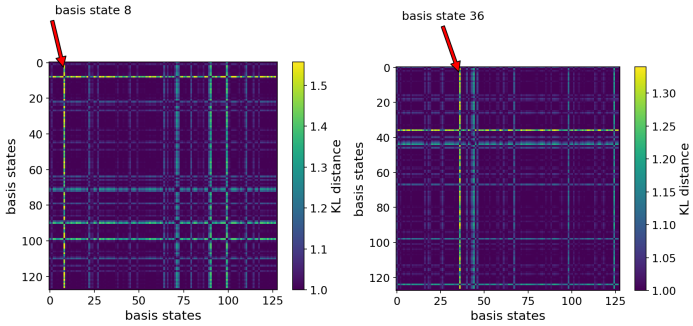

(a) IBM Nairobi (b) IBM Perth

Fig. 3: Pairwise KL-distance for all images inference jobs from IBM Nairobi and IBM Perth. Here we can see annotated state 8 for IBM Nairobi and state 36 for IBM Perth are yellow colored.

histograms. The resulting 128×128 KL-divergence matrix is rendered as a heat map in Figure 2a (ii), where blue denotes low divergence (high shape similarity) and yellow indicates high divergence (large shape differences). Several basis states most notably states 30 and 61 produce pronounced yellow lines, signifying that their error-distribution shapes differ markedly from those of the other basis states.

(5) **Low-Dimensional Embedding (Figure 1c):** Next, we embed each basis state's high-dimensional noise distribution (dimension $r = 8000$; see Figure 1c) into a two-dimensional space using Multidimensional Scaling (MDS) [12]. MDS seeks a 2D arrangement that preserves the previously computed pairwise KL-divergences, so basis states with similar error distribution shapes cluster together while dissimilar ones separate. The resulting map, shown in Figure 2a (iii), reveals that states 30 and 61 sit conspicuously far from the main cluster, and from one another exactly echoing the pronounced yellow bands associated with those states in the KL-divergence heat map (Figure 2a (ii)).

(6) **Clustering in a Projected Space (Figure 1d):** After embedding the basis states in two dimensions, we group those with similar error distributions via k-means clustering (Figure 1d). The optimal number of clusters K is chosen with the elbow method. We plot the distortion score the sum of squared distances from each state to its nearest centroid against K and select the knee of the curve in Figure 2b (i) [2]. The resulting clusters, displayed in distinct colours in Figure 2b (ii), reveal coherent groups of basis states. Notably, states 4, 20, 40, and 56 belong to the same purple cluster; their almost identical violin plots in Figure 2b (iii) corroborate that our low-dimensional embedding and k-means procedure robustly assemble states with highly similar noise distribution shapes.

(7) **Violin Plots and Classification of Noisy and Less-Noisy States (Figure 1e-f):** Finally, we visualize the error distributions of the cluster centroids derived from the k-means clustering using violin plots (see Figure 1e-f). As illustrated in Figure 2c (i), each violin plot represents the error distribution and the variance observed across the r rows of the raw data (denoted as "variance" on the y-axis of the violin plot). The violin plots effectively elucidate the distinctions between noisy and less

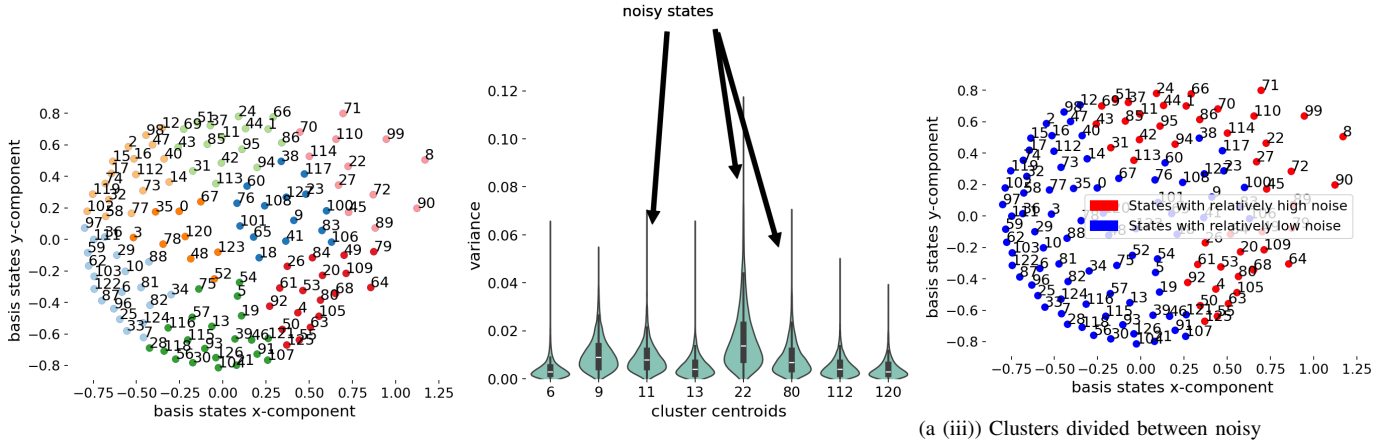

(a (i)) Basis states divided among 8 clusters

(a (ii)) Violin plots for cluster centroids

(a (iii)) Clusters divided between noisy and less noisy groups w.r.t variance

Fig. 4: IBM Nairobi: We repeat the process depicted in Figure 2 for visualization of noisy basis states. In particular, we first compute KL distances, low-dimensional projections, and optimal number of clusters for k-means algorithm (not depicted here). We then visualize noise distributions of cluster centroids (for clusters portrayed with different colors in a(i)) using violin plots (image a(ii)). We again segment the basis states projected in a scatterplot space (image a(iii)) based on relatively high variance (red) and low variance (blue). Our visualizations, therefore, facilitate quick insight into noisy and less-noisy basis states through compact visual representation.

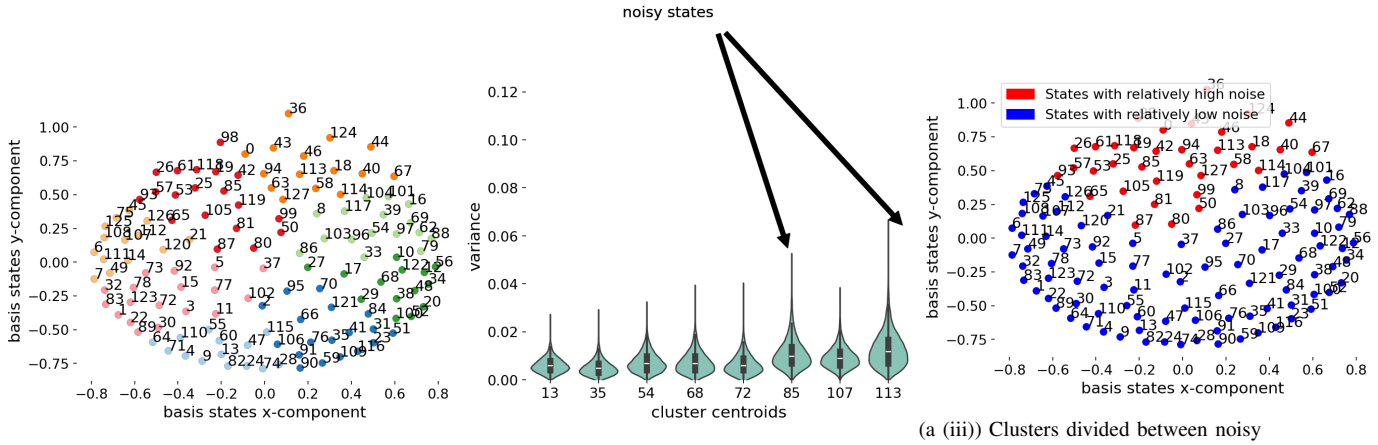

(a (i)) Basis states divided among 8 clusters

(a (ii)) Violin plots for cluster centroids

(a (iii)) Clusters divided between noisy and less noisy groups w.r.t variance

Fig. 5: IBM Perth: We repeat the same procedure for IBM Nairobi, as shown in Figure 4, to get the plots shown here.

noisy states on a cluster-by-cluster basis through their visual representation of noise distributions and variability. Notably, the centroid basis states 50, 61, and 105 in Figure 2c (i) exhibit a comparatively higher variance (indicating greater noise across r rows) than centroid basis states 22 and 117.

Our proposed violin plot approach, as depicted in Figure 2c (i), successfully addresses the visual clutter and clarity challenges associated with functional boxplots shown in Figure 2a (i). The violin plots concisely represent the diverse noise distributions within the raw data for the cluster centroids.

To provide a comprehensive assessment of noisy states, we further isolate members of the cluster centroids exhibiting relatively high noise in the MDS scatterplot, based on observations from the violin plots presented in Figure 2c (i). In Figure 2c (ii), we depict all basis states associated with cluster centroids 50, 61, and 105 in red, signifying those with relatively high noise. Conversely, all states from the remaining clusters are shown in blue, indicating relatively low noise levels. This is corroborated by Figure 2c (iii), which demonstrates that the randomly selected basis states (13, 76, and 95) within the cluster centering on 22 exhibit similar noise distributions to that of the basis state 22. Through the aforementioned sequence of analyses, we have established a novel technique for visually distinguishing between noisy and less noisy quantum basis states.

III. Experimental Setup And Results

We demonstrate the efficacy of our proposed visualization pipeline in identifying and elucidating noisy and less noisy quantum states. In Figure 2, we present results obtained from the IBM Lagos machine for class 3 images. We will subsequently detail the results for class 3 images from IBM Nairobi and IBM

Perth. The raw data matrix, as previously mentioned, retains the dimensions $r \times 128$, where $r = 8000$.

Figure 3, Figure 4, and Figure 5 collectively illustrate the outcomes for 128 basis states corresponding to the class 3 images from IBM Nairobi and IBM Perth. The functional boxplot approach [21] has been excluded from both IBM Nairobi and Perth analyses due to its demonstrated lack of clarity, consistent with the observations for IBM Lagos illustrated in Figure 2a (i). These plots do not reveal any significant visualization patterns due to information overload; however, functional boxplots serve as a useful preliminary method for understanding the noise distribution of basis states.

Consistent with Figure 2a (ii), we compute and visualize the pairwise Kullback-Leibler (KL) divergence among the error distributions of the basis states for class 3 images from IBM Nairobi and Perth, depicted in Figure 3. The calculated KL distance metrics are integral to the MDS projection step of our pipeline. A higher KL distance indicates a greater degree of disparity between two distribution shapes, while a lower KL distance reflects a closer similarity. For instance, the yellow coloration representing states 8 and 36 in the KL maps (see Figure 3a and Figure 3b) signifies a significant mismatch relative to other basis states.

We visualize the low-dimensional embedding of basis state distributions using MDS (with KL divergence as the dissimilarity metric) for both IBM Nairobi and Perth in Figure 4a (i) and Figure 5a (i), respectively. The low-dimensional embedding reveals that state 8 is spatially distanced from other states in Figure 4a (i), corroborating the yellow coloration indicating greater distribution dissimilarity observed in the KL-distance plot. This finding parallels state 30 from IBM Lagos, as depicted in Figure 2b (ii). Similarly, for IBM Perth, state 36 also appears spatially isolated from other states in Figure 5a (i), consistent with its yellow coloration. Thus, our MDS approach, based on KL divergence metrics, reliably preserves proportional spatial distances among basis states in a low-dimensional context.

Next, we apply k-means clustering to group states with analogous error distribution shapes, as indicated by distinct colors in Figure 4a (i) and Figure 5a (i). For both IBM Nairobi and Perth, we observe that the distortion scores converge after eight clusters, mirroring our previous findings in Figure 2b (i).

We visualize the noise distribution of the cluster centroid states using our proposed violin plots in Figure 4a (ii) and Figure 5a (ii). For IBM Nairobi, as shown in Figure 4a (ii), clusters with centroids 11, 22, and 80 exhibit relatively higher variance, indicating greater noise across the $r = 8000$ rows of the raw data compared to other clusters. Figure 4a (iii) and Figure 5a (iii) further delineate the noisy basis states corresponding to the identified clusters (i.e., centroids 11, 22, and 80) in red within the MDS scatterplot, thereby providing a comprehensive view of states characterized by relatively higher or lower noise levels. Similar to our observations for IBM Lagos in Figure 2c (iii), we note that states from clusters identified as noisy in both IBM Nairobi and Perth exhibit significant noise levels with comparable distributions. In summary, our proposed violin plot and MDS scatterplot visualizations afford enhanced insight into basis state noise, characterized by reduced visual clutter and improved clarity compared to functional boxplots.

Our visualization scheme can also serve as a diagnostic tool for spotting qubits with elevated noise. That information is valuable for both quantum error mitigation and circuit layout strategies: by flagging the noisiest hardware qubits, developers can steer their algorithms away from them when mapping circuits to a quantum processor. In quantum machine learning pipelines, for example, our visualizations help practitioners avoid assigning critical logical qubits to hardware qubits that would otherwise degrade classification or prediction accuracy.

IV. Conclusion

We present a new visualization framework that helps to classify noisy vs. less-noisy basis states and provide insight into basis-state noise distribution in quantum applications, focusing on Quantum Machine Learning (QML). Functional box plots [21] provide an initial view of noise in basis states but lead to a visual clutter, thereby impeding analysis. To overcome this issue, we present an advanced visualization pipeline to clearly provide insight into noisy and less-noisy basis states. In particular, our pipeline computes pairwise KL divergence, embeds data in 2D using MDS with KL metrics as a noise distribution symmetry measure, clusters projected basis states via k-means clustering, and displays cluster centroid noise distributions with violin plots. In future, we plan to investigate extension of our work to visually pinpoint noisy qubits for enhanced noise analysis and extend our ideas to other quantum applications.

V. Future Directions

Our pipeline is a self contained suite of Python scripts that consumes nothing but raw measurement data, either shot-by-shot readouts or aggregated CSV counts exported from Qiskit [11]. A user need only execute the circuits, save the counts, and point the script to the results directory; the code then analyzes the entire Quantum Machine Learning (QML) circuit family automatically. We are extending the tool beyond the Qiskit ecosystem and broadening its reach to both variational (e.g., Variational Quantum Eigen Solver (VQE), Variational Quantum Linear SOlver (VQLS)) and non-variational algorithms (e.g., phase estimation), while scaling to larger NISQ devices. Higher qubit counts will reveal richer effects intricate noise propagation, multi qubit interference, and evolving activation patterns that our visualizations can expose and help manage, ultimately enabling robust, large scale quantum machine-learning and computation.

VI. Code And Data Availability

The full repository containing all source code and every plot referenced in this paper is publicly available at https://github.com/psenap/QSW_Quantum_Visualization.git.

VII. ACKNOWLEDGMENTS

This work is supported in part by the NSF grants 402163, 402169, 402173 and the U.S. Department of Energy (DOE) RAPIDS SciDAC project under contract number DE-AC05-00OR22725.

REFERENCES

[1] A. S. Aasen, A. Di Giovanni, H. Rotzinger, A. V. Ustinov, and M. Gärttner. Readout error mitigated quantum state tomography tested on superconducting qubits. *Communications Physics*, 7(1):301, 2024.

[2] B. Bengfort and R. Bilbro. Yellowbrick: Visualizing the Scikit-Learn Model Selection Process. 4(35), 2019. doi: 10.21105/joss.01075

[3] D. Brahmbhatt, Y. Xu, N. Vora, L. Chen, N. Fruitwala, G. Huang, Q. Ji, and P. Nguyen. Qubicsv: An open-source data storage and visualization platform for collaborative qubit control. *arXiv e-prints*, pp. arXiv–2403, 2024.

[4] A. A. Clerk, M. H. Devoret, S. M. Girvin, F. Marquardt, and R. J. Schoelkopf. Introduction to quantum noise, measurement, and amplification. *Rev. Mod. Phys.*, 82:1155–1208, Apr 2010. doi: 10.1103/RevModPhys.82.1155

[5] S. Dasgupta and T. S. Humble. Reproducibility in quantum computing. In *2021 IEEE Computer Society Annual Symposium on VLSI (ISVLSI)*, pp. 458–461, 2021. doi: 10.1109/ISVLSI51109.2021.00090

[6] L. K. Grover. A fast quantum mechanical algorithm for database search. In *Proceedings of the twenty-eighth annual ACM symposium on Theory of computing*, pp. 212–219, 1996.

[7] R. Hicks, B. Kobrin, C. W. Bauer, and B. Nachman. Active readout-error mitigation. *Physical Review A*, 105(1):012419, 2022.

[8] J. L. Hintze and R. D. Nelson. Violin plots: a box plot-density trace synergism. *The American Statistician*, 52(2):181–184, 1998.

[9] D. Huber and S. J. Glaser. Beads: A canonical visualization of quantum states for applications in quantum information processing. *arXiv preprint arXiv:2410.01446*, 2024.

[10] E. Hyyppä, A. Vepsäläinen, M. Papič, C. F. Chan, S. Inel, A. Landra, W. Liu, J. Luus, F. Marxer, C. Ockeloen-Korppi, S. Orbell, B. Tarasinski, and J. Heinsoo. Reducing leakage of single-qubit gates for superconducting quantum processors using analytical control pulse envelopes. *PRX Quantum*, 5:030353, Sep 2024. doi: 10.1103/PRXQuantum.5.030353

[11] A. Javadi-Abhari, M. Treinish, K. Krsulich, C. J. Wood, J. Lishman, J. Gacon, S. Martiel, P. D. Nation, L. S. Bishop, A. W. Cross, B. R. Johnson, and J. M. Gambetta. Quantum computing with Qiskit, 2024. doi: 10.48550/arXiv.2405.08810

[12] J. B. Kruskal. Multidimensional scaling by optimizing goodness of fit to a nonmetric hypothesis. *Psychometrika*, 29(1):1–27, 1964.

[13] N. Li, F. Yan, and K. Hirota. Quantum data visualization: A quantum computing framework for enhancing visual analysis of data. *Physica A: Statistical Mechanics and its Applications*, 599:127476, 2022.

[14] Á. Márton and J. K. Asbóth. Coherent errors and readout errors in the surface code. *Quantum*, 7:1116, Sept. 2023. doi: 10.22331/q-2023-09-21-1116

[15] M. Richter, S. Lange, A. Bäcker, and R. Ketzmerick. Visualization and comparison of classical structures and quantum states of 4d maps. *arXiv preprint arXiv:1307.6109*, 2013.

[16] S. Ruan, Q. Guan, P. Griffin, Y. Mao, and Y. Wang. Quantumeyes: Towards better interpretability of quantum circuits. *IEEE Transactions on Visualization and Computer Graphics*, p. 1–13, 2024. doi: 10.1109/tvcg.2023.3332999

[17] S. Ruan, Y. Wang, W. Jiang, Y. Mao, and Q. Guan. Vacsen: A visualization approach for noise awareness in quantum computing. *IEEE Transactions on Visualization and Computer Graphics*, 1912.

[18] S. Ruan, Y. Wang, W. Jiang, Y. Mao, and Q. Guan. Vacsen: A visualization approach for noise awareness in quantum computing. *IEEE Transactions on Visualization and Computer Graphics*, 29(1):462–472, 2022.

[19] S. Ruan, R. Yuan, Q. Guan, Y. Lin, Y. Mao, W. Jiang, Z. Wang, W. Xu, and Y. Wang. Venus: A geometrical representation for quantum state visualization. In *Computer Graphics Forum*, vol. 42, pp. 247–258. Wiley Online Library, 2023.

[20] M. Sarovar, T. Proctor, K. Rudinger, K. Young, E. Nielsen, and R. Blume-Kohout. Detecting crosstalk errors in quantum information processors. *Quantum*, 4:321, 2020. doi: 10.22331/q-2020-09-11-321

[21] P. Senapati, T. M. Athawale, D. Pugmire, and Q. Guan. Advancing comprehension of quantum application outputs: A visualization technique. In *Proceedings of the 2023 International Workshop on Quantum Classical Cooperative*, pp. 25–28, 2023.

[22] P. Senapati, S. Y.-C. Chen, B. Fang, T. M. Athawale, A. Li, W. Jiang, C. C. Lu, and Q. Guan. Pqml: Enabling the predictive reproducibility on nisq machines for quantum ml applications. In *2024 IEEE International Conference on Quantum Computing and Engineering (QCE)*, vol. 01, pp. 1413–1424, 2024. doi: 10.1109/QCE60285.2024.00168

[23] P. Senapati, Z. Wang, W. Jiang, T. S. Humble, B. Fang, S. Xu, and Q. Guan. Towards redefining the reproducibility in quantum computing: A data analysis approach on NISQ devices. In *2023 IEEE International Conference on Quantum Computing and Engineering (QCE)*, vol. 1, pp. 468–474. IEEE, 2023.

[24] P. W. Shor. Algorithms for quantum computation: discrete logarithms and factoring. In *Proceedings 35th annual symposium on foundations of computer science*, pp. 124–134. Ieee, 1994.

[25] V. Tripathi, H. Chen, M. Khezri, K.-W. Yip, E. Levenson-Falk, and D. A. Lidar. Suppression of crosstalk in superconducting qubits using dynamical decoupling. *Phys. Rev. Appl.*, 18:024068, Aug 2022. doi: 10.1103/PhysRevApplied.18.024068

VIII. APPENDIX

We further demonstrate the effectiveness of our visualizations in classification of noisy and less noisy states for the class 6 and class 9 images for IBM Lagos, IBM Nairobi, and IBM Perth in Figure 6-Figure 11. These figures also demonstrate the visualization of noisy and less-noisy basis states/clusters involved in test image prediction through colormapping of our proposed MDS scatterplots and violin plots. The results shown in this section are in addition to the results shown in the section III section.

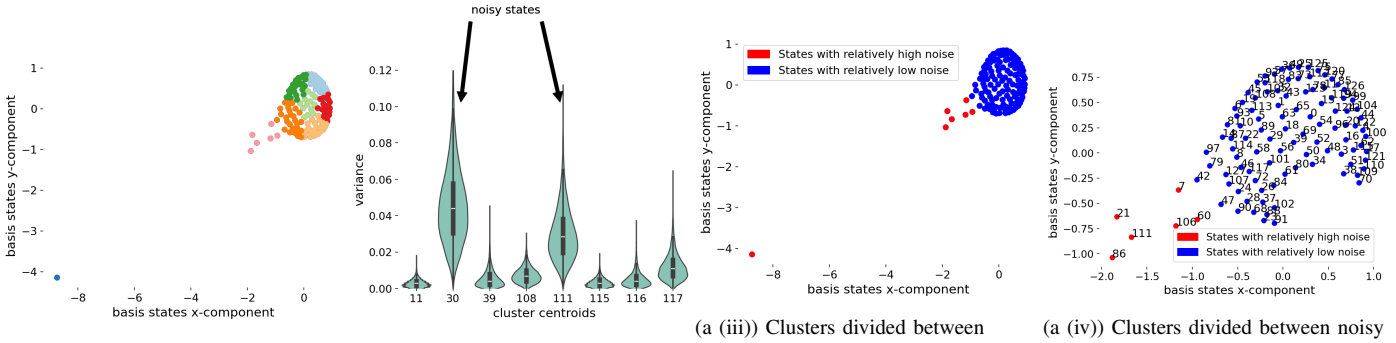

(a (i)) Basis states divided among 8 clusters

(a (ii)) Violin plots for cluster centroids

(a (iii)) Clusters divided between noisy and less noisy groups w.r.t variance

(a (iv)) Clusters divided between noisy and less noisy groups w.r.t variance and zoomed without state 30

Fig. 6: IBM Lagos: Class 6 Images. We repeat the same procedure for IBM Nairobi, as shown in Figure 4, to get the plots shown here. The annotations on the computational-basis states in panels a(i) and a(iii) have been omitted to enhance readability.

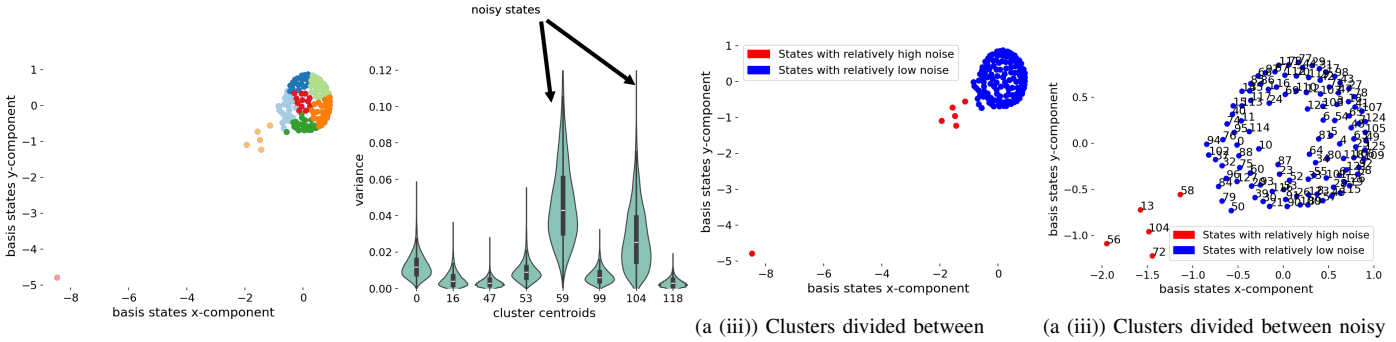

(a (i)) Basis states divided among 8 clusters

(a (ii)) Violin plots for cluster centroids

(a (iii)) Clusters divided between noisy and less noisy groups w.r.t variance

(a (iii)) Clusters divided between noisy and less noisy groups w.r.t variance and zoomed without state 30

Fig. 7: IBM Lagos: Class 9 Images. We repeat the same procedure for IBM Nairobi, as shown in Figure 4, to get the plots shown here. The annotations on the computational-basis states in panels a(i) and a(iii) have been omitted to enhance readability.

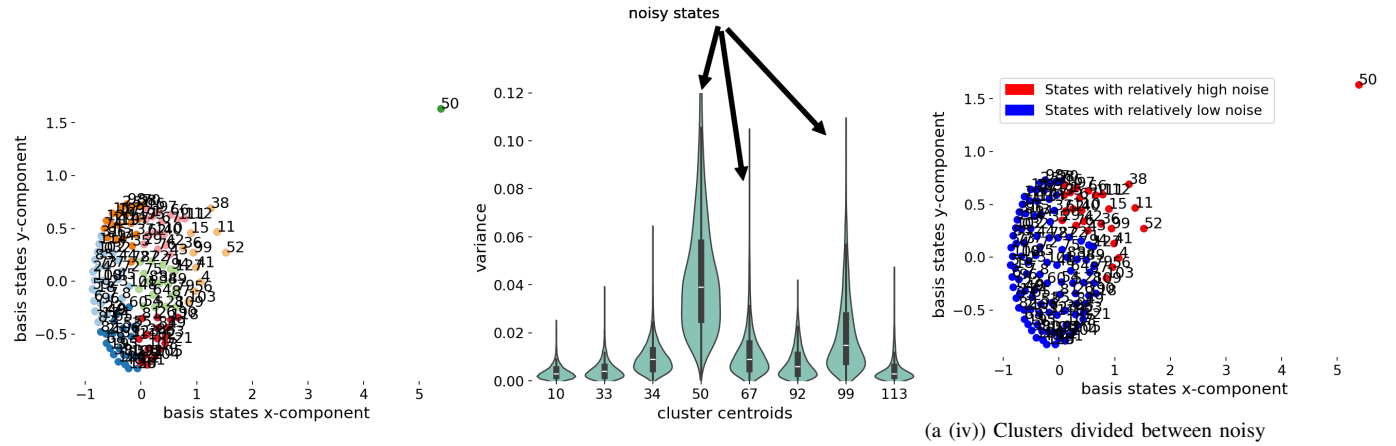

(a (i)) Basis states divided among 8 clusters

(a (ii)) Violin plots for cluster centroids

(a (iv)) Clusters divided between noisy and less noisy groups w.r.t variance.

Fig. 8: IBM Nairobi: Class 6 Images. We repeat the same procedure for IBM Nairobi, as shown in Figure 4, to get the plots shown here.

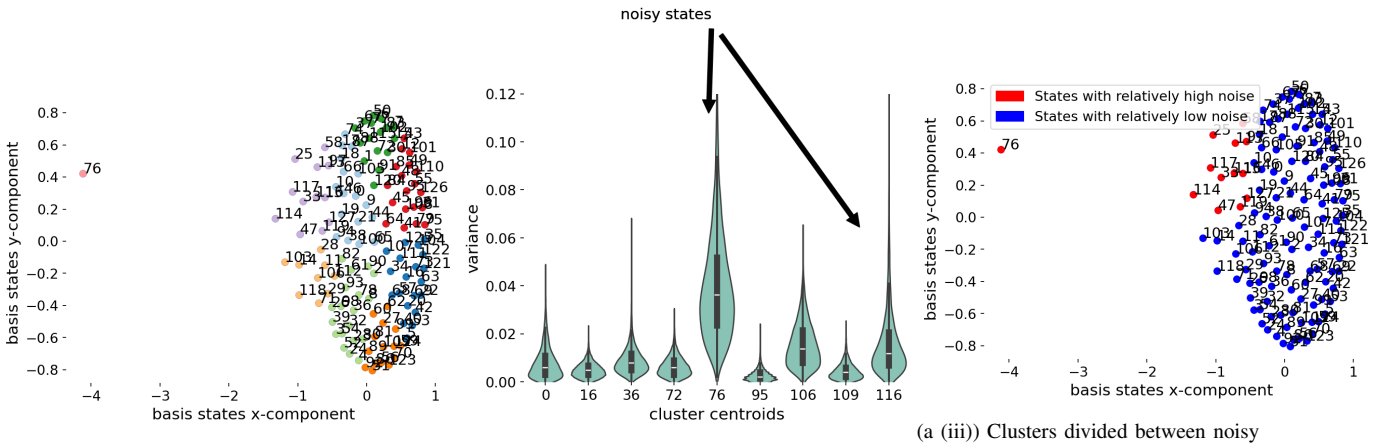

(a (i)) Basis states divided among 9 clusters

(a (ii)) Violin plots for cluster centroids

(a (iii)) Clusters divided between noisy and less noisy groups w.r.t variance

Fig. 9: IBM Nairobi: Class 9 Images. We repeat the same procedure for IBM Nairobi, as shown in Figure 4, to get the plots shown here.

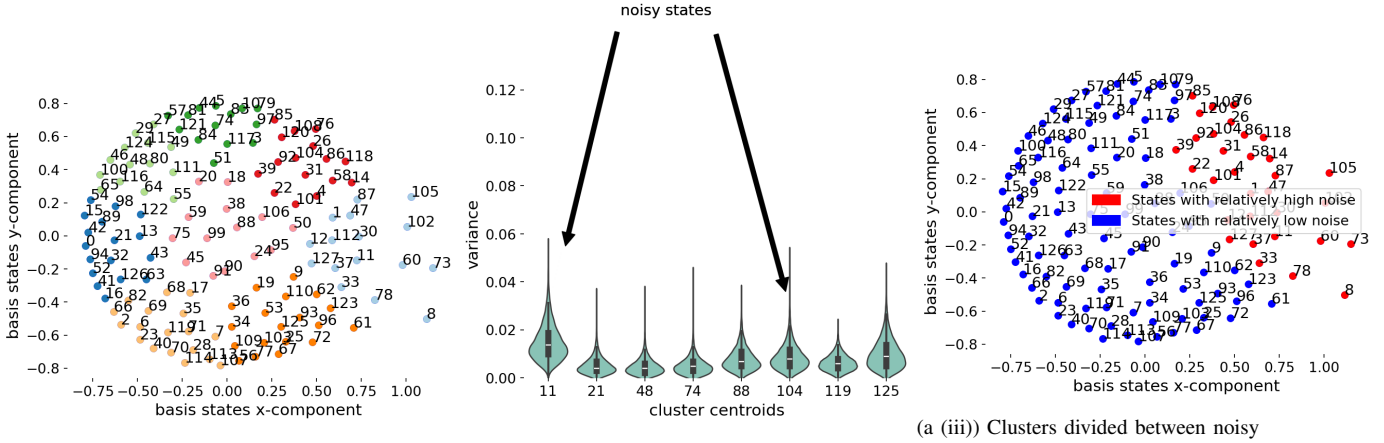

(a (i)) Basis states divided among 8 clusters

(a (ii)) Violin plots for cluster centroids

(a (iii)) Clusters divided between noisy and less noisy groups w.r.t variance

Fig. 10: IBM Perth: Class 6 Images. We repeat the same procedure for IBM Nairobi, as shown in Figure 4, to get the plots shown here.

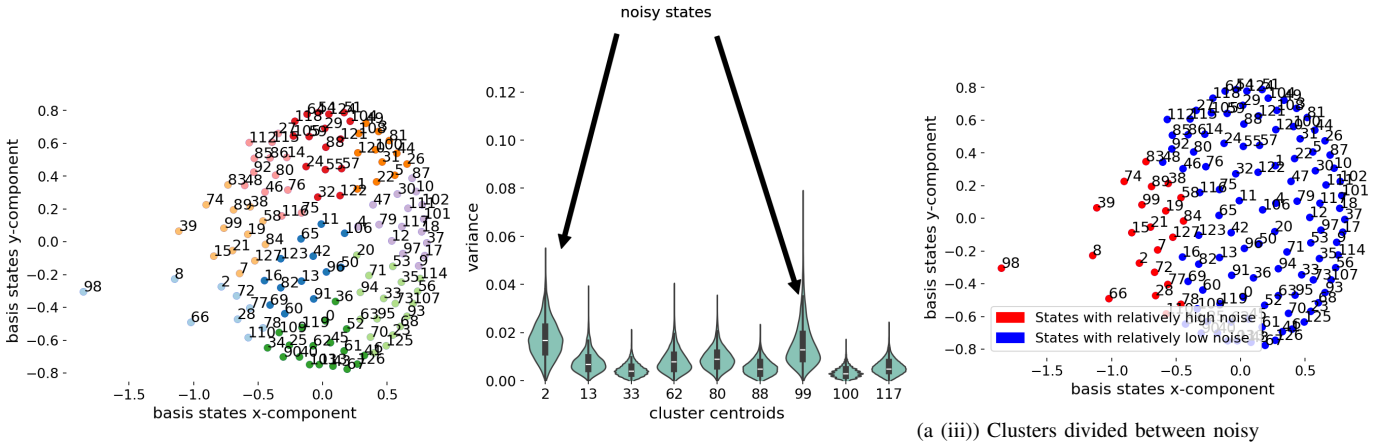

(a (i)) Basis states divided among 9 clusters

(a (ii)) Violin plots for cluster centroids

(a (iii)) Clusters divided between noisy and less noisy groups w.r.t variance

Fig. 11: IBM Perth: Class 9 Images. We repeat the same procedure for IBM Nairobi, as shown in Figure 4, to get the plots shown here.